ARTICLE

Chemically Linked AuNP–Alkane Network for Enhanced Photoemission and Field Emission

Xian Ning Xie,[†,*] Xingyu Gao,[‡] Dongchen Qi,[‡] Yilin Xie,[‡] Lei Shen,[§] Shuo-Wang Yang,[§] Chorng Haur Sow,[‡] and Andrew Thye Shen Wee[†,‡,*]

[†]NUS Nanoscience and Nanotechnology Initiative (NUSNNI), National University of Singapore, [‡]Department of Physics, National University of Singapore, 2 Science Drive 3, Singapore 117542, and [§]Institute of High Performance Computing, 1 Fusionopolis Way, Singapore 138632

ABSTRACT Size and ligand effects are the basis for the novel properties and applications of metallic nanoparticles (NPs) in nanoelectronics, optoelectronics, and biotechnology. This work reports the first observation of enhanced photoelectron emission from metallic Au NPs ligated by alkanethiols. The enhancement is based on a conceptually new mechanism: the AuNP provides electrons while the alkane ligand emits electrons due to its low or negative electron affinity. Moreover, the AuNP–ligand chemical bonding is found to significantly facilitate the transmission of photoexcited electrons from the AuNP to the ligand emitter. Consequently the smooth NP film, which is a typical low-aspect-ratio two-dimensional structure, exhibits strong and stable field emission behavior under photoillumination conditions. The photoenhanced field emission is related to the interband and surface plasmon transitions in AuNPs, and a photoenhancement factor of up to ~300 is observed for the AuNP-based field emission. This is highly remarkable because field emission is often based on one-dimensional, high-aspect-ratio nanostructures (*e.g.*, nanotubes and nanowires) with geometrical field enhancement effect. The chemical linkage of electron-supplying AuNP and electron-emitting alkane ligand represents a fundamentally new mechanism for efficient photoexcitation and emission. Being low-temperature/solution processable, and inkjet printable, AuNPs may be a flexible material system for optoelectronic applications such as photodetection and photoenhanced field emission.

KEYWORDS: gold nanoparticles · nanoparticle-ligand chemical bonding · photoemission · field emission · photodetection · photoassisted field emission · AuNP–alkane network

*Address correspondence to phyweets@nus.edu.sg, nnixxn@nus.edu.sg.

Received for review May 24, 2009 and accepted July 29, 2009.

Published online August 5, 2009. 10.1021/nn9005335 CCC: $40.75

Au nanoparticles (AuNPs) are usually passivated by ligands, and the physical and chemical effects associated with the NP-ligand system have been the focus of many works.[1–6] The NP-ligand chemical bonding is of particular importance because it is related to numerous unusual behaviors of NPs such as induced magnetic moments[7,8] and the screening of Coulomb blockade effect.[9] Alkanethiols are the most common ligands used for the passivation of AuNPs, and in most cases they are self-assembled on the NP surface through the Au–S covalent bond.[10,11] Much work has been devoted to the size and ligand effects on the electronic, thermal, and optical properties of NPs,[1–11] while no report on the photoelectron generation and emission from metallic AuNPs is available in the literature. Enhanced electron emission is usually observed for wide band gap (WBG) materials including diamond crystals and diamondoid molecules.[12–14] Because of the WBG, the conduction band (CB) edge is positioned above the vacuum level E_{vac}, so they exhibit negative electron affinity (NEA)[12–14] that facilitates electron emission into the vacuum without energy barrier. Metals like Au are good electron sources as there is a large population of conduction electrons near their Fermi level E_F. However, the Fermi level E_F of Au is 4.5–5.2 eV below E_{vac};[15,16] such a large energy barrier hinders electron emission to the vacuum, and therefore Au is not an electron-emitting material. On the other hand, alkanes are reported to be of low/negative electron affinity (LEA/NEA).[17–19] But their large HOMO–LUMO gap (≥8.0 eV[20,21]) renders them electrically insulating, and consequently there is no report on the application of alkanes as electron emitters.

This work reports the photoelectron emission behavior arising from the combination of AuNPs and alkane ligands. We demonstrate for the first time that when AuNPs are ligated with alkanes through Au–S chemical bonding, the nanocomposite exhibits enhanced photoelectron emission. The emission mechanism is based on the electron-providing function of AuNP and the electron-emitting characteristic of the NEA alkane. In the following paragraphs, we present photoelectron spectroscopy (PES) results to show the enhanced emission of secondary electrons (SEs) from the chemically bound AuNP-alkane ligand network. We then present DFT (density

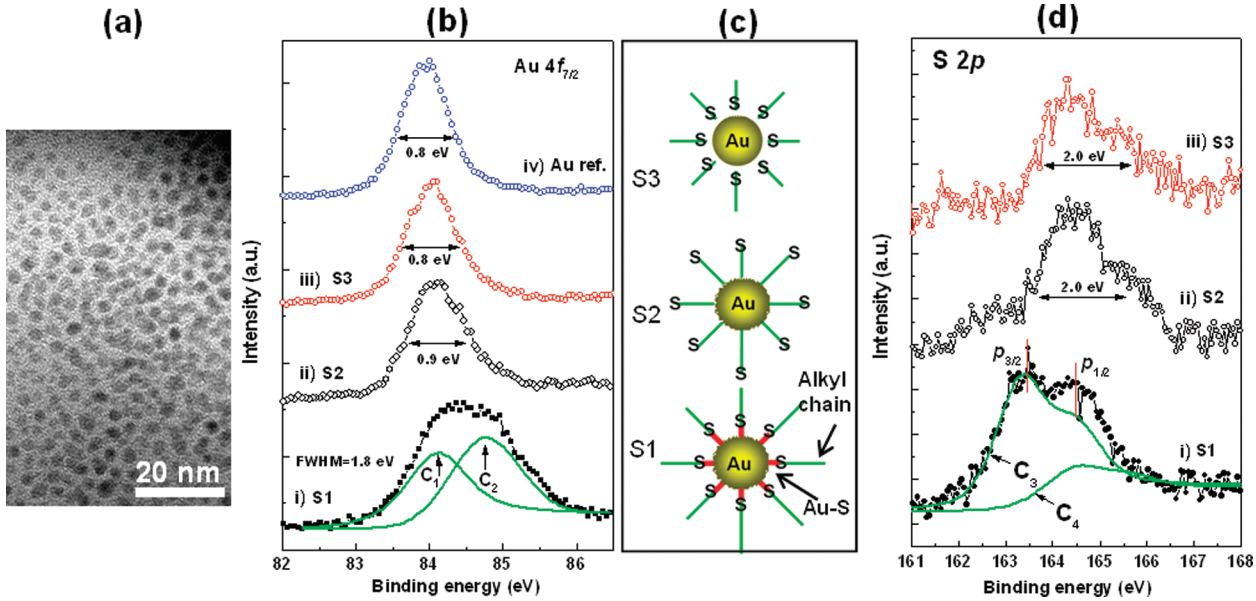

Figure 1. (a) Typical TEM (transmission electron microscope) image of S1 and S2 AuNP samples with an average diameter of 3.3 nm; (b) Au 4f PES spectra collected for AuNP samples S1, S2, and S3, respectively; (c) schematics showing the existence of Au−S bonding in S1, nonexistence of Au−S bonding in S2, and the thermal breakage of Au−S bond in S3, respectively; (d) corresponding S 2p PES spectra recorded for samples S1−S3, respectively. Photons with energy of 560 eV were used in PES measurements.

functional theory) calculation to elucidate the photoemission mechanism and highlight the role of Au−S bonding in facilitating the NP→ligand SE transmission. Due to the photoenhancement effect, strong and stable field emission is observed for the AuNP film under photoillumination conditions. The variation of photoenhancement factor as a function of photon energy and power density is discussed, and the unique features of AuNP-based photoenhanced field emission are compared with those of geometry-enhanced field emission typical of conventional nanostructures.

RESULTS AND DISCUSSION

We first compare the PES results among AuNP samples S1−3 with and without Au−S bonding at the NP-ligand interface, respectively. The AuNP samples S1 and S2 used in this work were chemically synthesized according to an early publication[4] (see Supporting Information section *i* for experimental). Sample S1 AuNP is passivated by 11-mercaptoundecanoic acid [MUA, $HS-(CH_2)_{10}-COOH$] ligand and is water-soluble; sample S2 AuNP is capped by 11-mercaptoundecanol [MUO, $HS-(CH_2)_{10}-CH_2-OH$] ligand and is soluble in methonal. Despite the different solubility caused by ligand terminal groups, the S1 and S2 AuNPs are of the same average diameter of 3.3 nm (see Figure 1a), and exhibit similar electric conductivity of $10^{-7}-10^{-6}$ S/cm.[4] In this work, our PES (see Supporting Information section *ii* for experimental details) results reveal that the AuNP−ligand interface is different between the two samples: S1 is characterized by the formation of Au−S chemical bonding, while there is no such Au−S bonding in S2. As shown in Figure 1b, the Au $4f_{7/2}$ PES peak of S1 is very broad with a fwhm (full width at half-maximum) of 1.8 eV. The fwhm is much larger than that of 0.8 eV recorded for a Au reference film shown as spectrum iv in Figure 1b. The broad peak of sample S1 is deconvoluted into two components C_1 and C_2. Component C_1 is located at the same position (~84.0 eV) as the peak of the Au reference, and therefore is attributed to the unbound inner Au atoms in the NP. Component C_2 is located at a higher binding energy of ~84.8 eV, and is associated with Au−S bond formation.[10,11] The corresponding S2p peak of S1 (see spectrum i in Figure 1d) is also quite broad (fwhm = 2.7 eV), and exhibits two components: C_3 with $2p_{3/2}$ = 163.4 eV and $2p_{1/2}$ = 164.5 eV; C_4 with $2p_{3/2}$ = 164.3 eV and $2p_{1/2}$ = 165.4 eV. The former with a lower binding energy is due to the Au−S bonding, while the latter is attributed to S atoms not participating in the Au−S bond formation.[22,23] In contrast, the Au $4f_{7/2}$ peak of sample S2 (see spectrum ii in Figure 1b) is much narrower (fwhm = 0.9 eV) and is positioned around 84.0 eV, indicating that sample S2 is bulk-like without the formation of Au−S bonds at the AuNP−ligand interface. Consequently, the S2p peak of sample S2 (see spectrum ii in Figure 1d) is narrower (fwhm = 2.0 eV), and only contains a single component of unbound S atoms. PES survey scan shows that the C1s:Au$4f_{7/2}$:S2p peak intensity ratio observed for samples S1 and S2 is almost the same (see Supporting Information section iii), indicating nearly identical AuNP/ligand chemical stoichiometry between the two samples. The above results suggest that the AuNP−ligand interface can be either chemically or physically linked. In Figure 1c, we propose that the formation of chemical and physical interface is due to the orientation of the ligand relative to the AuNP surface. For sample S1, the thiol group is

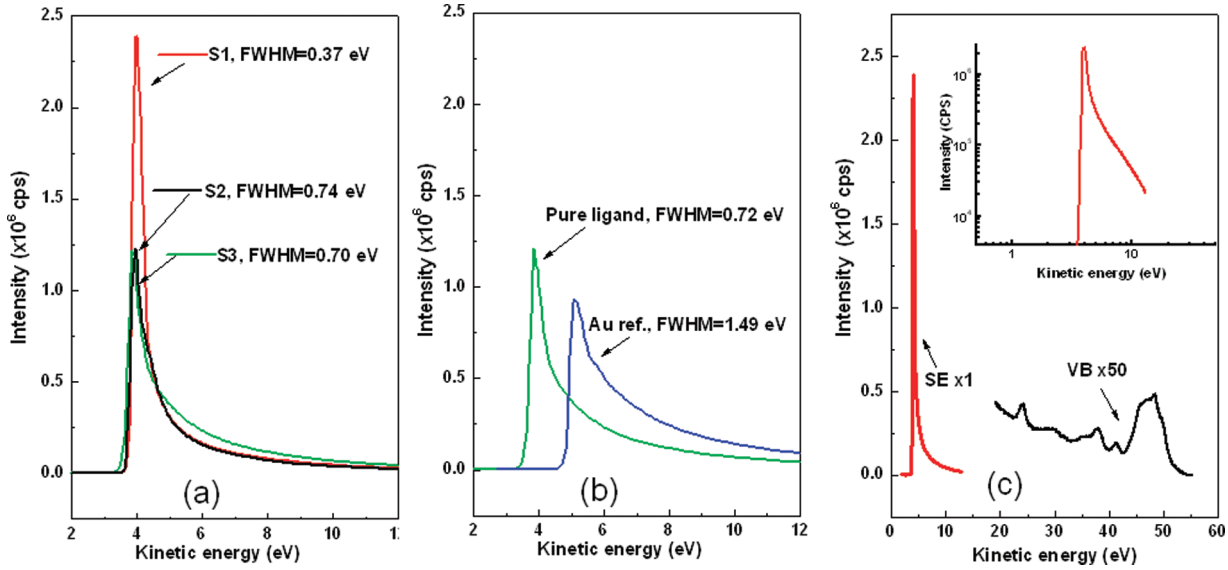

Figure 2. (a) Comparison of secondary electron (SE) emission intensity among samples S1−3; (b) the SE intensity of pure MUA ligand film and Au reference film are also shown in comparison with that shown in panel a; (c) comparison of SE intensity and valence band (VB) intensity of sample S1. The inset shows the log−log plot of the SE peak. All the spectra were collected under identical conditions in the PES experiments. Photons with energy of 60 eV were used for the above measurements.

facing the AuNP, and this configuration facilitates the formation of Au−S bonding. In the case of sample S2, however, the thiol terminal group is facing outside, and the alkane ligand is only physisorbed on the AuNP surface. Such physisorption and unbound S atoms have been observed[23−25] for alkylthiol self-assembly on Au surfaces (*e.g.*, see Figure 9 in ref 25), and are found to be sensitive to the wet-chemistry molecular assembly conditions such as the solvent used and the times of rinsing the assembled layers. In the case of physisorption, the individual AuNPs are still passivated by the ligands, and the AuNP surface is stabilized by the ligand through physical effects such as van der Waals interaction and Pauli repulsion. That is, the electron cloud of the ligand pushes back the spill-out electrons of the AuNPs, and the AuNP/ligand interface is dominated by van der Waals interaction.[26] Here, we believe the difference in Au−S bonding between S1 and S2 samples is caused during the reduction of Au^{3+} to Au^0 by sodium borohydride (see Supporting Informationsection *i*). In this process, the AuNP is being formed and the surrounding alkylthiol ligands subsequently absorb on the NP surface. So the difference in reaction temperature and duration, and solution stirring conditions of this key step would affect the AuNP−ligand interface formation. In addition to wet-chemistry approach, we found that the physical interface can also be formed by breaking the Au−S bonds of samples S1 through the thermal annealing of S1 in vacuum around ≤100 °C for a few minutes (the annealed sample is referred to as S3). The Au $4f_{7/2}$ and S2p spectra of sample S3 are displayed Figure 1 panels b and d, respectively. It is seen that both peaks are similar to those of sample S2, indicating the cleavage of Au−S bond by thermal annealing in vacuum. Moreover, the C1s: Au $4f_{7/2}$: S2p of sample S3 is also very close to that of samples S1 and S2 (see Supporting Information section iii). This indicates that under the above annealing condition, only the Au−S bond is cleaved, while the evaporation of the ligand molecule is negligible (see Figure 1c for the proposed interface structure of S3). Y. Kim, R. C. Johnson, and J. T. Hupp[5] performed NMR (nuclear magnetic resonance) measurements of MUA passivated AuNPs, and they found that the α-carbon atom of MUA is not detectable because of its closest proximity to the AuNP core (see Figure S1 in ref 5). It would be instructive to do similar NMR characterizations for our samples S1−3 and find out if the Au−S bonding affect the detection of the α-carbon atom. Although the chemical composition of the AuNP samples S1−S3 are similar, the photoemission behavior of them, as demonstrated below, exhibits a strong dependence on the existence of Au−S interfacial bonding.

Figure 2a exhibits the secondary electron (SE) emission spectra collected for samples S1−3, respectively. For sample S1 with Au−S bonding, a sharp and narrow emission peak located at 4.0 eV dominates the spectrum. The peak intensity reaches 2.4×10^6 cps (counts per second), and its fwhm is only 0.37 eV. From the low-kinetic energy cutoff of the SE peak, the work function of the AuNP film is determined to be $W_F = 3.8$ eV. In contrast, under identical PES experimental conditions, the peak intensity of sample S2 without Au−S bonding is only 1.2×10^6 cps, and its fwhm broadens to 0.74 eV. The SE peak intensity and fwhm of sample S3, in which the Au−S bonding has been thermally cleaved, are almost identical to those of sample S2 (see Figure 2a). This result indicates that the Au−S bonding significantly facilitates SE emission from the ligated AuNPs to the vacuum. In comparison, the SE intensity observed

for pure MUA ligand film and Au reference film is shown in Figure 2b. It can be seen that the peak position, intensity, and fwhm of the pure ligand film are similar to those of samples S2 and S3. We suggest that in sample S1, both the AuNP and ligand are contributing to SE emission: the SEs from AuNP are transmitted to ligand through Au−S bonds, thus leading to enhanced SE emission. Since there are no Au−S bonds in samples S2 and S3, the SEs generated in AuNPs cannot be transmitted to the ligands for emission, therefore only the ligand is involved in SE emission. This is why the SE emission of the pure ligand is also similar to that of samples S2 and S3. For the Au reference film, the broad peak (fwhm = 1.49 eV) is a result of the wide energy distribution of secondary electrons emitted from its continuous conduction band. The low-kinetic energy cutoff of the peak is 4.9 eV, in agreement with the work function W_F = 4.5−5.2 eV reported for bulk Au.[15,16] The fwhm of sample S1 is only 25% that of the Au reference. The sharp SE peak of S1 can be attributed to the LEA/NEA[17−19] of the alkane ligand. It is reported that LEA/NEA greatly enhances SE emission, such that the SE peak intensity is usually much higher than that of the valence band (VB) electrons.[12−14] In the case of the AuNP sample S1 with Au−S bonding, the SE intensity is 250 times that of the VB electron (see Figure 2c). The sharp SE peak is even clearly visible in the log−log plot shown in the inset of Figure 2c, which exhibits the exponential decay typical of secondary emission.

We propose a three-step mechanism to explain the higher SE intensity observed in Figure 2 for sample S1 with Au−S bonding. First, the valence electrons of the AuNP are photoexcited into its CB where they thermalize to form secondary electrons. Second, the secondary electrons are transmitted to the unoccupied orbitals of the ligand by Au−S bonding. Third, the secondary electrons are emitted from the LUMO of the ligand to the vacuum, and the emission is enhanced due to the LEA/NEA of the alkane ligand. To provide a more detailed description on how the Au−S bonding facilitates the AuNP → ligand SE transfer, we conducted DFT (density functional theory; see Supporting Information section *iv* for details on model construction and simulations) to examine the NP−ligand chemical interface and electronic configuration. Figure 3a shows the AuNP model containing a Au38 cluster chemically bonded to six SH-$C_{11}H_{23}$ alkane ligands *via* Au−S bonds. A NEA of 0.41 eV was calculated for the alkane ligand, in agreement with previous observations.[17−19] The Au−S bonding is characterized by the strong overlap of charge density between Au and S atoms as shown in Figure 3b. The calculation reveals that one S atom interacts with three surface Au atoms to form an optimal tetrahedron configuration, in agreement with previous results.[27] The bonding is characterized by the strong overlap of charge density between Au and S atoms. Here, only two Au atoms are visible on the charge density map because the third one is blocked in this direction of view. The Au−S bonding has a crucial effect on the NP/ligand interface electronic configuration. As displayed in Figure 3c, in the absence of Au−S bonding, there is no overlap between the DOS of AuNP and ligand in the energy range from E_F to the LUMO of ligand, and this configuration hinders the transmission of SEs from AuNP to ligand. In contrast, substantial DOS are generated at the interface by the Au−S bonding as demonstrated in Figure 3d. Here, instead of the total DOS, we selectively highlight the partial DOS which is involved in the Au−S bonding and is thus significant to SE transmission. It can be seen that the Au 6p, 6s, and 5d states form the CB of AuNP 0−4.5 eV above E_F, and these states overlap (or are coupled) with the S 3p state in the same energy range. This continuous subband is induced by the Au−S bonding, and it links the AuNP CB and the empty states of the alkane chain, thus creating an energy window (0−4.5 eV wide) which facilitates the AuNP → ligand transmission of SEs. Very strong Au 5d state is observed 0−8.0 eV below E_F, whose maximum DOS is calculated to be ~10 times that of the Au 6s state. The Au 6sp electrons are responsible for the intraband excitation, while the filled Au 5d state below E_F provides large number of electrons for the 5d → 6sp interband transition under photon illumination conditions. It is clear in Figure 3d that the SE in AuNPs can be transmitted to the ligand through the highly hybridized Au 5d, 6sp and S 3p states. Note that the CB DOS shown in Figure 3d corresponds to the existence of six Au−S bonds at the NP−ligand interface. When more Au−S bonds are formed, the density of the overlapped states above E_F would increase significantly, and accordingly the SE transmission would be more energetically favored. Figure 3e provides a pictorial description of the photoelectron transfer and emission from AuNPs with Au−S bonding at the NP−ligand interface.

The enhanced photoelectron emission is further confirmed by our field emission (FE) experiments. Figure 4a displays the FE current obtained for samples S1−3 under the illumination of 405 nm light (power density = 40 mW/cm^2). The experimental setup of the photoenhanced FE measurements is shown in the inset of Figure 4a (see Supporting Information section *v* for details). It can be seen that only sample S1 exhibits FE current with a turn-on field of F = 5.7 V/μm, starting from which, the FE current increases sharply from 1.1 × 10^{-9} to 8.5 × 10^{-6} A (or 0.28 mA/cm^2 in current density) at F = 11 V/μm. As justified later, such exponential current increase by three orders is typical of Fowler−Nordheim (FN) field emission. In contrast, the *IV* curves observed for samples S2 and S3, respectively, in Figure 4a do not exhibit this turn-on behavior, indicating the absence of FE characteristic in the samples. Without light illumination, the *IV* curves observed for samples S1, S2, and S3, respectively, all resemble the

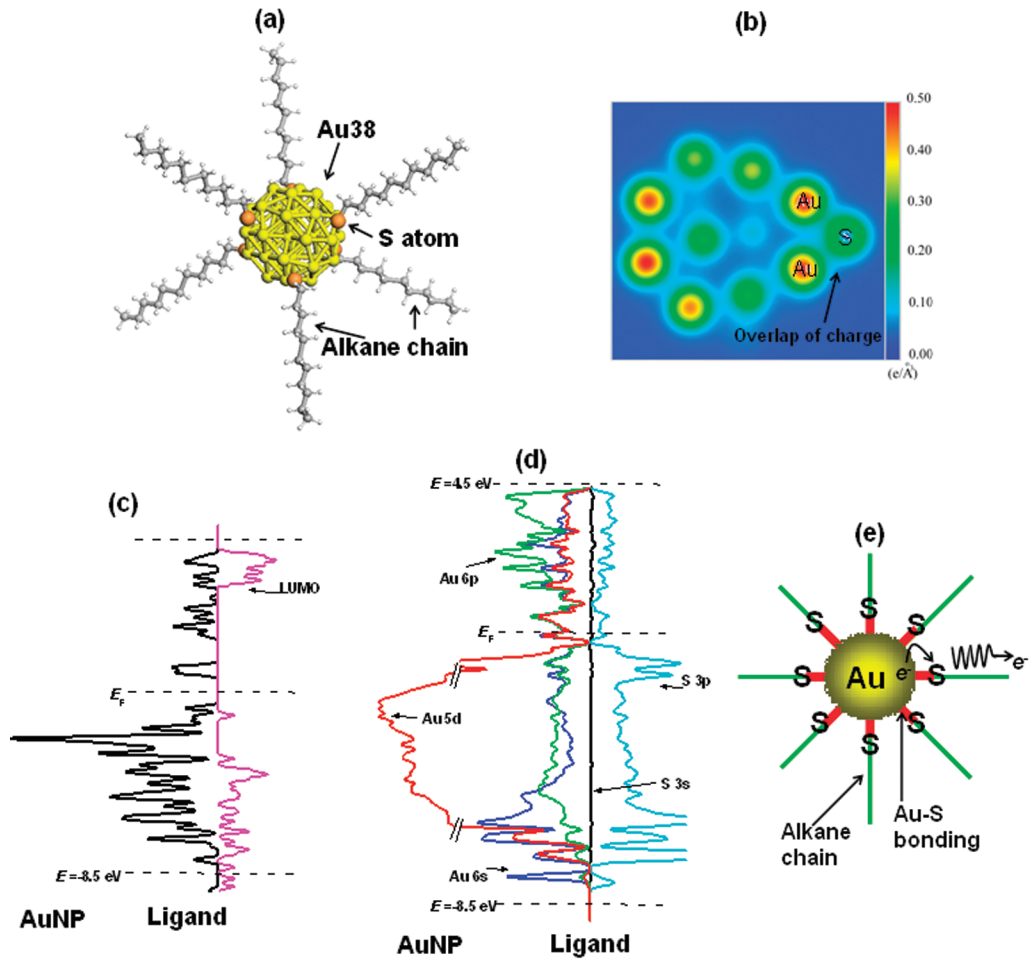

Figure 3. (a) The AuNP model consisting of a Au38 cluster and six alkanethiol molecules chemically bound to the cluster through Au−S bonds; (b) charge distribution showing the overlap of charge density between Au and S atoms; (c) total DOS calculated for the Au NP/ligand interface without Au−S bonding; (d) orbital specific partial-DOS calculated for the AuNP/ligand interface with Au−S bonding; (e) pictorial illustration of the transmission of SE from AuNP to alkane ligand and the emission of SE by the NEA ligand.

one labeled as "Dark current" in Figure 4a. The observation indicates that the FE current is photoactivated and is only generated in sample S1 with Au−S bonding. This is in agreement with the three-step mechanism proposed for photoemission in the preceding paragraph in which the Au−S bonding facilitates the transmission of photoelectrons from the NP to ligand. To further address the photoassisted FE current, the *IV* curve of sample S1 was fitted to the FN field emission equation in its commonest format[28,29]

$$\ln\left(\frac{I}{F^2}\right) = -\frac{BW_F^{3/2}}{\beta}\frac{1}{F} + \ln\left(\frac{A\gamma\beta}{W_F}\right) \qquad (1)$$

where I (in A) is the FE current, F (in V/cm) the electric field, W_F (in eV) the work function of the sample, β the enhancement factor, and γ (in cm^2) the emitting area. A and B are two constants with $A = 1.4 \times 10^{-6}(\mathrm{A \cdot eV \cdot V^{-2}})$, and $B = 6.44 \times 10^7(\mathrm{V \cdot cm \cdot eV^{-3/2}})$, respectively.[29] Equation 1 dictates a linear relation between ln (I/F^2) and ($1/F$) for FE current. In Figure 4b, the same *IV* of sample S1 shown in Figure 4a obtained under light illumination is plotted in the FN format. It can be seen the *IV* obeys the FN equation, and the best-fit to eq 1 is ln (I/F^2) = $-1.5 \times 10^6/F - 19.6$, in which the slope of -1.5×10^6 corresponds to $-BW_F^{3/2}/\beta$. Using $W_F = 3.8$ eV determined in Figure 2a by PES, an enhancement factor of $\beta = 301$ is obtained for the photoenhanced FE of AuNP sample S1. Note that in FE, β is usually a measure of the field enhancement caused by the geometry of emitters, and large β values are often associated with sharp emitter structures with high aspect ratios. Consequently, FE is only observed for 1D nanostructures such as nanotubes, nanowires, and nanorods.[30−36] Since our AuNP film is a very smooth 2D surface with a rms (root-mean-square) roughness of 0.62 nm (see Supporting Information section *vi*), the enhancement due to sharp geometry should not exist on such a flat surface. Therefore, the large enhancement of $\beta = 301$ observed in Figure 4b can be fully attributed to the photoenhancement effect. This observation is quite remarkable as it implies that large scale FE can be achieved on the basis of photoenhancement by using a flat NP film prepared with simple spin-coating

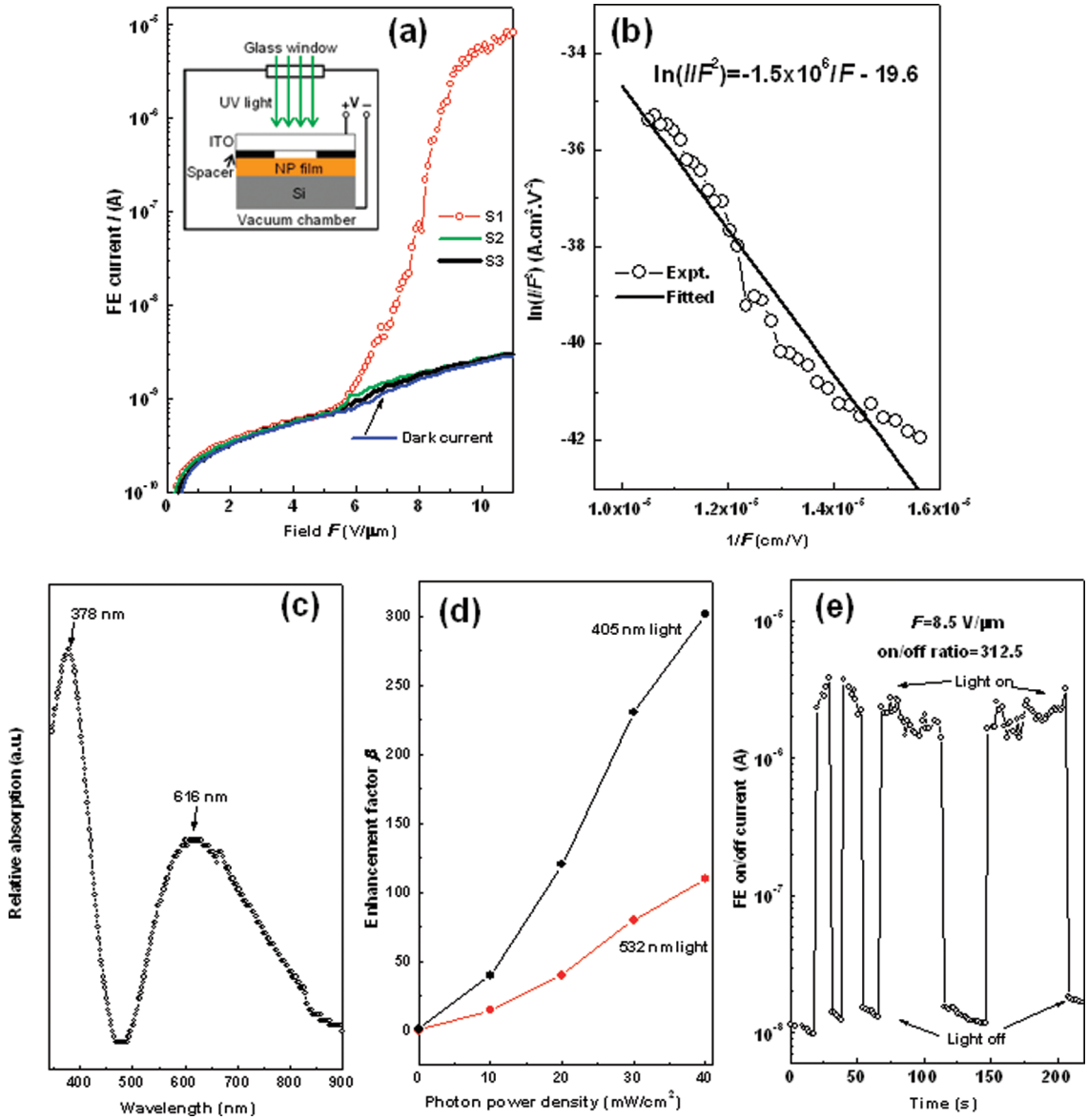

Figure 4. (a) Comparison of FE current of samples S1−3 under 405 nm light (40 mW/cm^2) illumination. The typical *IV* (or dark current) of the samples obtained without light illumination is also shown. The inset shows the FE experimental setup. (b) Experimental and fitted FN plots of the same FE current of samples S1 shown in panel a; (c) optical absorption spectrum collected for AuNP sample S1; (d) variation of enhancement factor β of sample S1 as a function of the power density of light used in FE experiments; 405 and 532 nm lights were used respectively to illuminate the sample; (e) on/off FE current observed for sample S1 when alternatively switching on and off the 405 nm@40 mW/cm^2 light.

method. This approach may provide an alternative to FE based on high-aspect-ratio nanostructures. In the latter case, the uniformity and areal density of FE depends on the distribution and vertical alignment of individual nanostructures, and the control of these factors requires delicate preparation and multiple patterning steps.

Figure 4c displays the optical absorption spectrum recorded for AuNP sample S1 (see Supporting Information section *vii*). Two prominent absorption peaks are observed at 378 and 616 nm, respectively. The short wavelength peak is due to the Au 5d → 6sp interband transition, while the long wavelength absorption corresponds to the well-known surface plasmon (SP) excitation.[37,38] In Figure 4c, the interband peak is stronger than the SP peak, and this is caused by the enhancement of interband transition when the size of noble metals is reduced to the nanoscale.[37] As displayed in Figure S3 (see Supporting Information section *vii*), the SP peak of individual AuNPs is located at ~540 nm, in agreement with previous observations.[1−3] But for the film composing closely packed AuNPs, the SP peak is red-shifted to 616 nm. This is because the close-packing of AuNPs causes the inter-NP coupling effect, such that the absorption of the film is not just a simple summation of that of individual AuNPs. Instead, the collective effect of interacting NPs in the film also contributes significantly to the overall absorption of the AuNPs

assembly,[39−41] thus leading to the large redshift observed in Figure 4c. In the literature, such redshift has been observed for metallic NP aggregates and is attributed to the multipole coupling between closely positioned NPs.[40,41] The broad SP absorption observed in Figure 4c is in agreement with the SP excitation observed for the same MUA- or MUO-passivated AuNPs reported earlier (see Figure 4 in ref 4). In Figure 4a, 405 nm light is used for photoexcitation, so the photoelectrons are generated by the enhanced interband transition in AuNPs. In addition, the energy of the 405 nm light ($h\nu = 3.1$ eV) is too low to excite electrons from the ligand with a gap of ≥8.0 eV (note the SE peaks observed for S2, S3, and pure ligand film in Figure 2 panels a and b are due to the large photon energy of 60 eV used in PES measurements). This unambiguously indicates that all the emitted electrons are from the AuNPs, and the FE current in Figure 4(a) is fully composed of photogenerated electrons. According to Figure 3(d) and (e), the photoemission involves the excitations of ANP electrons to form SEs, and the subsequent transmission SEs to the unoccupied orbitals of the ligand. On the basis of the transfer matrix formula,[42,43] one can derive an explicit relation between FE current I and the number $N(E)$ of excited electrons and the interface transmission probability $P(E)$:

$$I = I_0(T)\, P(E)\, N(E) \qquad (2)$$

where $I_0(T)$ is a temperature T dependent constant, while $N(E)$ and $P(E)$ are functions of electron energy E (see Supporting Information section *viii*). No FE is observed in Figure 4a without light illumination because there are no SEs with an energy higher than E_F, and the 0−11 V/μm field strength is insufficient to electrically emit electrons. This scenario corresponds to a near-zero $P(E)N(E)$ production in eq 2, and thus a zero FE current. With light illumination, a large amount of SEs with energies above E_F is generated in the CB of AuNPs, thus leading to a large $N(E)$ value. Moreover, the strong coupling of the Au 6p, 6s, and 5d states with the S 3p state associated with Au−S bonding significantly improves the transmission probability $P(E)$ of the NP/ligand interface. Therefore, both the number of electron $N(E)$ and transmission probability $P(E)$ in eq 2 are substantially increased, and this combined effect is responsible for the FE behavior observed for sample S1 shown in Figure 4a,b). The energy E of photoexcited electrons is in the broad range of $E_F \le E \le E_F + h\nu$. At a low field F, only a small portion of electrons with a higher energy close to $E_F + h\nu$ are emitted. This stage corresponds to the turn-on of FE at $F = 5.7$ V/μm shown in Figure 4a. When F is increased, more and more photoelectrons with a lower energy of $E \ge E_F$ are emitted, and this is the origin of the rapid current increase by three orders in the FE regime of $F = 5.7-11$ V/μm shown in Figure 4a.

Figure 4d displays the variation of β as a function of the power density of photons used in FE experiments. When a photon of 405 nm@40 mW/cm^2 is used, a β of ~300 is obtained on the basis of eq 1. When the power density is reduced, the β value decreases, for example, β = 250 and 120 when the power density is 30 and 20 mW/cm^2, respectively. This observation is related to the number $N(E)$ of photoelectrons generated: a lower power density corresponds to a smaller $N(E)$ of photoelectrons, and thus a lower FE current according to eq 2. A similar change in β as a function of decreasing power density is also observed for 532 nm photons (see Figure 4d). The electron emission by the 532 nm light should be due to the AuNP SP excitation which spans a wide range of 500−900 nm as shown in Figure 4c. The FE enhancement (see Figure 4d) of the 532 nm light is smaller than that of the 405 nm light partly due to the lower photon energy (2.3 eV) of the former. Figure 4e displays the FE current variation of sample S1 under a constant field of $F = 8.5$ V/μm when the 405 nm@40 mW/cm^2 light was switched on and off alternately. It is seen that the FE is turned on and off instantly by the light, and the on/off current ratio reaches 312.5, much higher than that of <4 reported for semiconductor nanostructures.[32,33] In addition, the on/off current remains quite stable over prolonged (>200 s) light illumination. This good FE stability is in contrast to the quick decrease (*e.g.*, after ~5 s illumination) of the on/off ratio observed for CuO nanobelts. In the latter case, field emission depends on ionic carriers, and these carriers can often be desorbed by photon illumination, thus leading to the deterioration of FE property as widely observed for nanotubes and nanobelts.[32−34] In our experiments, the NP film was used for repeated FE measurements, reproducible *IV*s similar to that shown in Figure 4a,e were always obtained, and there was no sign of degradation by light illumination and field application. In addition, no obvious change in *IV* characteristics of the NP film was observed after storing the film in a drybox for >12 months. The result shown in Figure 4e demonstrates the high photosensitivity and good stability of AuNP film as a new material for photoemission and photodetection applications. In Figure 4a, the turn-on voltage and maximum FE current density of the AuNP field emitter is 570 V and 0.28 mA/cm^2, respectively. In comparison with those (200 V and 100 mA/cm^2, respectively)[30,31] of the well-known carbon nanotube (CNT) emitter, further work is needed to improve the FE performance of the AuNP emitter. However, the fabrication of AuNP film is low-temperature, solution processable, and is inkjet printable.[4] Moreover, the photoenhanced FE mechanism of AuNPs does not require a high aspect-ratio emitting structure as the 1D CNT does, and thus FE is possible on the flat AuNP film as demonstrated in Figure 4.

CONCLUSION

In conclusion, we have reported the first observation of enhanced photoemission from alkane-ligated metallic AuNPs. The AuNPs supply photoelectrons while the Au−S chemical bonding significantly improves the AuNP-ligand interface transmission probability, thus enhancing electron emission from the negative-electron-affinity ligand. Photoenhanced field emission by AuNP interband and surface plasmon excitations is demonstrated, and enhancement factor up to 300 is observed. The photoenhancement effect allows for large scale and stable field emission from a flat 2D NP film, in contrast to the usual field emission based on high-aspect-ratio 1D nanostructures. In view of its flexibility in preparation and device fabrication, the chemically ligated AuNPs may provide a new photoactive material for photoemission, photodetection, and field emission.

EXPERIMENTAL AND SIMULATION

All the chemicals used in the chemical synthesis of AuNPs were purchased from Aldrich. The synthesis of MUA- and MUO-passivated AuNPs is based on the method shown in ref 4. AuNPs films were deposited onto Si substrates by the spin-coating method. The samples were characterized by TEM (transmission electron microscope), optical absorption, PES (photoelectron spectroscopy), AFM (atomic force microscope). Field emission experiments were conducted with and without light illumination, respectively. DFT (density functional theory) simulation was also carried out to examine the AuNP−ligand interface. All the details about the above experimental and simulation work are provided in Supporting Information.

Acknowledgment. We gratefully thank Mr. S. Sivaramakrishnan and Dr. P. K.-H. Ho of the Organic NanoDevices Lab (ONDL, Physics Department at NUS) for kindly providing the AuNP samples and performing TEM and optical characterizations of the AuNPs. This work is supported by the NUS Nanoscience and Nanotechnology Initiative (NUSNNI), National University of Singapore.

Supporting Information Available: Chemical synthesis of Au NPs and spin-coating of NP films; PES characterization; PES survey spectra; DFT calculation; field emission experiments; AFM image of AuNP film; optical absorption spectrum of AuNP film; derivation of eq. 2. This material is available free of charge *via* the Internet at http://pubs.acs.org.

REFERENCES AND NOTES

1. Daniel, M.-C.; Astruc, D. Gold Nanoparticles: Assembly, Supramolecular Chemistry, Quantum-Size-Related Properties, and Applications towards Biology, Catalysis, and Nanotechnology. *Chem. Rev.* **2004**, *104*, 293–346.
2. Moriarty, P. Nanostructured Materials. *Rep. Prog. Phys.* **2001**, *64*, 297–381.
3. Baletto, F.; Ferrando, R. Structural Properties of Nanoclusters: Energetic, Thermodynamic, and Kinetic Effects. *Rev. Mod. Phys.* **2005**, *77*, 371–423.
4. Sivaramakrishnan, S.; Chia, P.-J.; Yeo, Y.-C.; Chua, L.-L.; Ho, P. K.-H. Controlled Insulator-to-Metal Transition in Printable Polymer Composites with Nanometal Clusters. *Nat. Mater.* **2007**, *6*, 149–154.
5. Kim, Y.; Johnson, R. C.; Hupp, J. T. Gold-Nanoparticle-Based Sensing of "Spectroscopically Silent" Heavy Ions. *Nano Lett.* **2001**, *1*, 165–167.
6. Hao, E.; Bailey, R. C.; Schatz, G. C.; Hupp, J. T.; Li, S. Synthesis and Optical Properties of "Branched" Gold Nanocrystals. *Nano Lett.* **2004**, *4*, 327–330.
7. Crespo, P.; Litran, R.; Rojas, T. C.; Multigner, M.; de la Fuente, J. M.; Sanchez-Lopez, J. C.; Garcia, M. A.; Hernando, A.; Penades, S.; Fernandez, A. Permanent Magnetism, Magnetic Anisotropy, and Hysteresis of Thiol-Capped Gold Nanoparticles. *Phys. Rev. Lett.* **2004**, *93*, 087204/1–087204/4.
8. Yamamoto, Y.; Miura, T.; Suzuki, M.; Kawamura, N.; Miyagawa, H.; Nakamura, T.; Kobayashi, K.; Teranishi, T.; Hori, H. Direct Observation of Ferromagnetic Spin Polarization in Gold Nanoparticles. *Phys. Rev. Lett.* **2004**, *93*, 116801/1–116801/4.
9. Medeiros-Ribeiro, G.; Ohlberg, D. A. A; Williams, R. S.; Heath, J. R. Rehybridization of Electronic Structure in Compressed Two-Dimensional Quantum Dot Superlattices. *Phys. Rev. B* **1999**, *59*, 1633–1636.
10. Zhang, P.; Sham, T. K. X-ray Studies of the Structure and Electronic Behavior of Alkanethiolate-Capped Gold Nanoparticles: The Interplay of Size and Surface Effects. *Phys. Rev. Lett.* **2003**, *90*, 245502/1–245502/4.
11. Sham, T. K.; Kim, P.-S. G.; Zhang, P. Electronic Structure of Molecular-Capped Gold Nanoparticles From X-ray Spectroscopy Studies: Implications for Coulomb Blockade, Luminescence and Non-Fermi Behavior. *Solid State Commun.* **2006**, *138*, 553–557.
12. Yang, W. L.; Fabbri, J. D.; Willey, T. M.; Lee, J. R. I.; Dahl, J. E.; Carlson, R. M. K.; Schreiner, P. R.; Fokin, A. A.; Tkachenko, B. A.; Fokina, N. A.; *et al.* Monochromatic Electron Photoemission from Diamondoid. *Science* **2007**, *316*, 1460–1462.
13. Pan L. S.; Kania, D. R. In *Diamond: Electronic Properties and Applications*; Kluwer Academic Publisher: Boston, MA, 1995.
14. Bell, R. L. In *Negative Electron Affinity Devices*; Clarendon: Oxford, U.K., 1973.
15. Koch, N. Organic Electronic Devices and Their Functional Interfaces. *ChemPhysChem* **2007**, *8*, 1438–1455.
16. Tanaka, A.; Imamura, M.; Yasuda, H. Interface Electronic Structure of Alkanethiolate-Capped Au Nanoparticles Studied by Photoelectron Spectroscopy. *Phys. Rev. B* **2006**, *74*, 113402/1–113402/4.
17. Sanche, L. see Chapter 1 in *Excess Electrons in Dielectric Media*; Ferradini. C., Jay-Gerin, J. P., Eds.; CRC Press: Boca Raton, FL, 1991.
18. Sanche, L. Transmission Through Organic Thin-Films. *Phys. Rev. Lett.* **1995**, *75*, 2904.
19. Righi, M. C.; Scandolo, S.; Serra, S.; Iarlori, S.; Tosatti, E.; Santoro, G. Surface States and Negative Electron Affinity in Polyethylene. *Phys. Rev. Lett.* **2001**, *87*, 076802/1–076802/4.
20. Boulas, C.; Davidovits, J. V.; Rondelez, F.; Vuillaume, D. Suppression of Charge Carrier Tunneling Through Organic Self-Assembled Monolayers. *Phys. Rev. Lett.* **1996**, *76*, 4797–4800.
21. Vuillaume, D.; Bouls, C.; Collet, J.; Daviddovist, J. V.; Rondelez, F. Organic Insulting Films of Nanometer Thickness. *Appl. Phys. Lett.* **1996**, *69*, 1646–1648.
22. Hu, M.; Yamaguchi, Y.; Okubo, T. Self-Assembly of Water-Dispersed Gold Nanoparticles Stabilized by a Thiolated Glycol Derivative. *J. Nanopart. Res.* **2005**, *7*, 187–193.
23. Castner, D. G.; Hinds, K.; Grainger, D. W. X-ray Photoelectron Spectroscopy Sulfur 2p Study of Organic Thiol and Disulfide Binding Interaction with Gold Surfaces. *Langmuir* **1996**, *12*, 5083–5086.
24. Yasseri, A. A; Syomin, D.; Malinovskii, V. L.; Loewe, R. S.; Lindsay, J. S.; Zaera, F.; Bocian, D. F. Characterization of Self-Assembled Monolayers of Porphyrins Bearing Multiple Thiol-Derivtized Rigid-Rod Tethers. *J. Am. Chem. Soc.* **2004**, *126*, 11944–11953.

25. Shirai, Y.; Cheng, L.; Chen, B.; Tour, J. M. Characterization of Self-Assembled Monolayers of Fullerene Derivatives on Gold Surfaces: Implications for Device Evaluations. *J. Am. Chem. Soc.* **2006**, *128*, 13479–13489.
26. Crispin, X.; Geskin, V.; Crispin, A.; Cornil, J.; Lazzaroni, R.; Salaneck, W. R.; Bredas, J.-L. Characterization of the Interface Dipole at Organic/Metal Interfaces. *J. Am. Chem. Soc.* **2002**, *124*, 8131–8141.
27. Hakkinen, H.; Barnett, R. N.; Landman, U. Electronic Structure of Passivated $Au_{38}(SCH_3)_{24}$ Nanocrystal. *Phys. Rev. Lett.* **1999**, *82*, 3264–3267.
28. Nicolaescu, D. Physical Basis for Applying the Fowler−Nordheim J−E Relationship to Experimental *IV* Data. *J. Vac. Sci. Technol., B* **1993**, *11*, 392–395.
29. Brodie, I.; Spindt, C. A. Vacuum Microelectronics. *Adv. Electron. Electron. Phys.* **1992**, *83*, 1–106.
30. De Heer, W. A.; Chatelain, A.; Ugarte, D. A Carbon Nanotube Field-Emission Electron Source. *Science* **1995**, *270*, 1179–1180.
31. De Heer, W. A.; Bonard, J. M.; Fauth, K.; Chatelain, A.; Forro, L.; Ugarte, D. Electron Field Emitters Based on Carbon Nanotube Film. *Adv. Mater.* **1997**, *9*, 87–89.
32. Zhu, Y. W.; Sow, C. H.; Thong, J. T. L. Enhanced Field Emission from CuO Nanowire Arrays by *in Situ* Laser Irradiation. *J. Appl. Phys.* **2007**, *102*, 114302/1–114302/7.
33. Chen, J.; Huang, N. Y.; Deng, S. Z.; She, J. C.; Xu, N. S. Effects of Light Illumination on Field Emission from CuO Nanobelt Arrays. *Appl. Phys. Lett.* **2005**, *86*, 151107/1–151107/3.
34. Chen, R. J.; Franklin, N. R.; Kong, J.; Cao, J.; Tombler, T. W. Molecular Photodesorption from Single-Walled Carbon Nanotubes. *Appl. Phys. Lett.* **2001**, *79*, 2258–2260.
35. Shim, M.; Siddons, G. P. Photoinduced Conductivity Changes in Carbon Nanotube Transistors. *Appl. Phys. Lett.* **2003**, *83*, 3564–3566.
36. Wang, W. Z.; Zeng, B. Q.; Yang, J.; Poudel, B.; Huang, J. Y.; Naughton, M. J.; Ren, Z. F. Aligned Ultralong ZnO Nanobelts and Their Enhanced Field Emission. *Adv. Mater.* **2006**, *18*, 3275–3278.
37. Balamurugan, B.; Maruyama, T. Evidence of an Enhanced Interband Absorption in Au Nanoparticles: Size-Dependent Electronic Structure and Optical Properties. *Appl. Phys. Lett.* **2005**, *87*, 143105/1–143105/3.
38. Hutter, E.; Fendler, J. H. Exploitation of Localized Surface Plasmon Resonance. *Adv. Mater.* **2004**, *16*, 1685–1706.
39. Kreibig, U.; Genzel, L. Optical-Absorption of Small Metallic Particles. *Surf. Sci.* **1985**, *156*, 678–700.
40. Shipway, A. N.; Lahav, M.; Gabai, R.; Willner, I. Investigation into the Electrostatically Induced Aggregation of Au Nanoparticles. *Langmuir* **2000**, *16*, 8789–8795.
41. Norman, T. J.; Grant, C. D.; Magana, D.; Zhang, J. Z.; Liu, J.; Cao, D.; Bridges, F.; Van Buuren, A. Near Infrared Optical Absorption of Gold Nanoparticle Aggregates. *J. Phys. Chem. B* **2002**, *106*, 7005–7012.
42. Wang, R. Z.; Ding, X. M.; Wang, B.; Xue, K.; Xu, J. B.; Yan, H.; Hou, X. Y. Structural Enhancement Mechanism of Field Emission from Multilayer Semiconductor Films. *Phys. Rev. B* **2005**, *72*, 125310/1–125310/6.
43. Tsu, R.; Esaki, L. Tunneling in a Finite Superlattice. *Appl. Phys. Lett.* **1973**, *22*, 562–564.